Self-Assembly

International Edition: DOI: 10.1002/anie.201813955
German Edition: DOI: 10.1002/ange.201813955

Interplay between H-Bonding and Preorganization in the Evolution of Self-Assembled Systems

Divya S. Philips, Kalathil K. Kartha, Antiope T. Politi, Timo Krüger, Rodrigo Q. Albuquerque, and Gustavo Fernández**

Abstract: *Cooperative π–π interactions and H-bonding are frequently exploited in supramolecular polymerization; however, close scrutiny of their mutual interplay has been largely unexplored. Herein, we compare the self-assembly behavior of a series of C_2- and C_3-symmetrical oligophenyleneethynylenes differing in their amide topology (N- or C-centered). This subtle structural modification brings about drastic changes in their photophysical and supramolecular properties, highlighting the reciprocal impact of H-bonding vs. preorganization on the evolution and final outcome of supramolecular systems.*

Numerous life processes including protein–ligand recognition, cell–cell interaction, and cytoskeletal formation are governed by the subtle interplay of multiple noncovalent interactions.[1] Among them, cooperative H-bonding and π–π interactions are overwhelmingly exploited for the construction of ordered arrays of artificial functional molecules.[2] This approach provides detailed structural and mechanistic insights into the underlying self-assembly pathways.[3] However, there is still a lack of fundamental understanding of the reciprocal influence of H-bonding and preorganization on molecular conformational changes preceding aggregation and the subsequent evolution into the final supramolecular structures.

Oligomeric π-systems[4] are promising building blocks to bridge this knowledge gap due to their variable torsional flexibility, which in turn allows versatile molecular reorganization upon aggregation. In this context, oligo(*p*-phenyleneethynylene)s (OPEs) represent a particularly relevant class of molecules with excellent optical and electronic properties, which have been extensively applied in the fields of optoelectronics,[5] sensors,[6] and stimuli-responsive materials.[7] OPEs have also been exploited to create hierarchical self-assembled structures driven by π-stacking and H-bonding.[8] Herein, we reveal how the subtle interplay between H-bonding and preorganization determines the evolution and final outcome of supramolecular nanostructures. To address this challenge, we compare the self-assembly behavior of a series of C_2- and C_3-symmetrical OPEs (**1**–**4**, Figure 1),

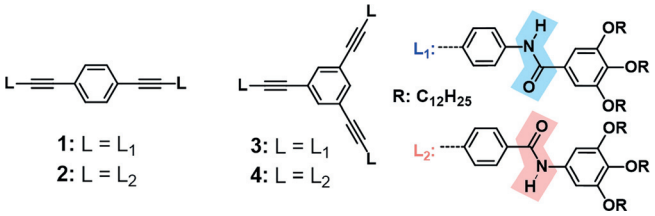

Figure 1. Chemical structures of OPEs **1**–**4**. The highlighted portions show the nature of amide connectivity (N-centered, blue; C-centered, pink).

differing only in the amide topology (N- or C-centered, for their synthesis see the Supporting Information). The investigations were first carried out on the linear OPEs (**1** and **2**), and these results were then compared with those obtained for the C_3-symmetrical derivatives (**3** and **4**) to confirm the generalization of the trends found.

Initial semiempirical calculations at the PM7 level indicate marked differences in the electron density distribution brought about by the inversion of the amide topology. While the highest occupied molecular orbital (HOMO) is delocalized over the aromatic core for the N-centered OPEs **1** and **3**, it is localized more on the peripheral phenyl rings for the C-centered derivatives **2** and **4** (Figures S1 and S2). On the other hand, the lowest unoccupied molecular orbital (LUMO) is largely localized on the central aromatic core for all molecules. These findings have two main implications: 1) a strong charge-transfer (CT) character for HOMO–LUMO excitations is expected for the C-centered systems, where the outer phenyl rings behave as donor units and the central aromatic core acts as the acceptor. This CT character can significantly affect the emission characteristics; 2) The N-centered molecules (**1**, **3**) show a much stronger HOMO–LUMO overlap than that of the C-centered counterparts (**2**, **4**), which is an indication of more allowed electronic transitions for the former OPEs. In fact, the absorption and

[*] Dr. D. S. Philips, Dr. K. K. Kartha, T. Krüger, Prof. Dr. G. Fernández
Organisch-Chemisches Institut
Westfälische Wilhelms-Universität Münster
Corrensstraße 40, 48149 Münster (Germany)
E-mail: fernandg@uni-muenster.de
A. T. Politi, Prof. Dr. R. Q. Albuquerque
School of Pharmacy and Biomolecular Sciences
Liverpool John Moores University (LJMU)
Liverpool (UK)
E-mail: ralbuque@uni-muenster.de
Prof. Dr. R. Q. Albuquerque
São Carlos Institute of Chemistry, University of São Paulo (Brazil)
Supporting information and the ORCID identification number(s) for the author(s) of this article can be found under: https://doi.org/10.1002/anie.201813955.

emission studies match well with the theoretical predictions. The molar absorptivity ε in a good solvent as chloroform ($CHCl_3$, $c = 1 \times 10^{-5}$ M) at the respective absorption maxima is ca. 35 % higher for **1** than for **2** (89 000 vs. 66 000 L mol^{-1} cm^{-1}, Figure S3 a,b) and about 45 % higher for **3** compared to **4** (140 000 vs. 95 000 L mol^{-1} cm^{-1}, Figure S4). The emission spectrum of **1** in $CHCl_3$ ($c = 1 \times 10^{-5}$ M, $\lambda_{ex} = 300$ nm) displayed two distinct vibronic transitions at 381 nm and 401 nm with almost equal intensities, while **2** was nearly non-emissive, probably due to charge transfer from the donor side groups to the acceptor core (Figure S3 d,e).[9] **4** was also nearly non-emissive compared to **3** for the same reason (Figures S7 and S9).

Significant differences in the optical properties caused by aggregation are observed for all molecules in a poor solvent such as methylcyclohexane (MCH). For **1**, variable-temperature (VT) UV/Vis studies at 1×10^{-4} M (for other experiments at various concentrations, see Figure S5) using a cooling rate of 1 K min^{-1} showed an initial enhancement in absorption when the temperature was decreased from 363 to 327 K along with a slight red-shift from 340 to 343 nm without any isosbestic point (Figure 2 a, inset).

Further cooling to 283 K revealed a 2 nm blue shift of the absorption maximum and the simultaneous appearance of a red-shifted broad contribution at 385 nm through clear isosbestic points at 265, 332, and 371 nm (Figure 2 a). Identical absorption changes upon aggregation were observed for the C_3-symmetrical N-centered homologue **3** (Figure S7 a). Emission studies of **1** showed a slight fluorescence enhancement when the temperature was decreased from 363 to 327 K followed by a significant quenching between 327 and 283 K (Figures 2 b and S6). The observed optical features between 363 and 327 K can be ascribed to the restricted molecular rotation of the OPE core,[10] which results in a coplanar π-backbone with improved conjugation leading to an increment in the absorbance and emission due to restriction of the non-radiative pathways. Below 327 K, the planarization-induced preorganization (Figure 2 d) ultimately promotes a subsequent aggregation event via aromatic interactions of the OPE units, as is evident from fluorescence and UV/Vis studies. For both N-centered OPEs **1** and **3**, the blue shift of the absorption maximum along with the appearance of a red-shifted shoulder are in accordance with a face-to-face stacking of the OPE units with a slightly twisted arrangement in order to favor H-bonding interactions. This is indeed supported by the PM7 geometry optimizations performed for hexameric stacks of **1** (Figure 2 c,d) and pentameric stacks of **3** (Figure S7 c,d). The calculations reveal a highly planar nature of the OPE cores within the stacks, which are stabilized by van der Waals interactions involving the chains, amide H-bonds, and aromatic interactions.

On the other hand, VT-absorption and fluorescence measurements of the C-centered OPEs in MCH gave rather different observations. Unlike **1**, **2** displays no increase in absorption, that is, no planarization on cooling from 363 to 313 K, but rather a concomitant decrease in intensity and red-shift from 335 to 338 nm (Figure 2 e; for an overview at various concentrations see Figure S8). Simultaneously, a red-shifted shoulder at 380 nm and a clear isosbestic point at 362 nm become evident. The lack of planarization is also found from PM7 calculations (see Figures 2 g,h) and can be attributed to the slight mismatch between H-bonds and aromatic interactions caused by the inversion in the amide topology, which results in a less compact packing of the OPE units. This is evident from the twisting and translational displacement of the π-backbones observed in the PM7-optimized hexameric stacks of **2** (Figure 2 g,h) and pentameric stacks of **4** (Figure S9 c,d), which is in agreement with the red-shift in the absorption upon aggregation. These experiments also reveal a gradual increase in absorbance but no changes in the spectral shape below 313 K (Figure 2 e), most likely indicating non-specific aggregation of the previously formed assemblies. The new shoulders observed in the low-temperature absorption spectra of **1** and **2** (380–385 nm) and of **3** and **4** (ca. 360 nm) were reproduced in the theoretical UV/Vis spectra predicted for small aggregates using the ZINDO/S

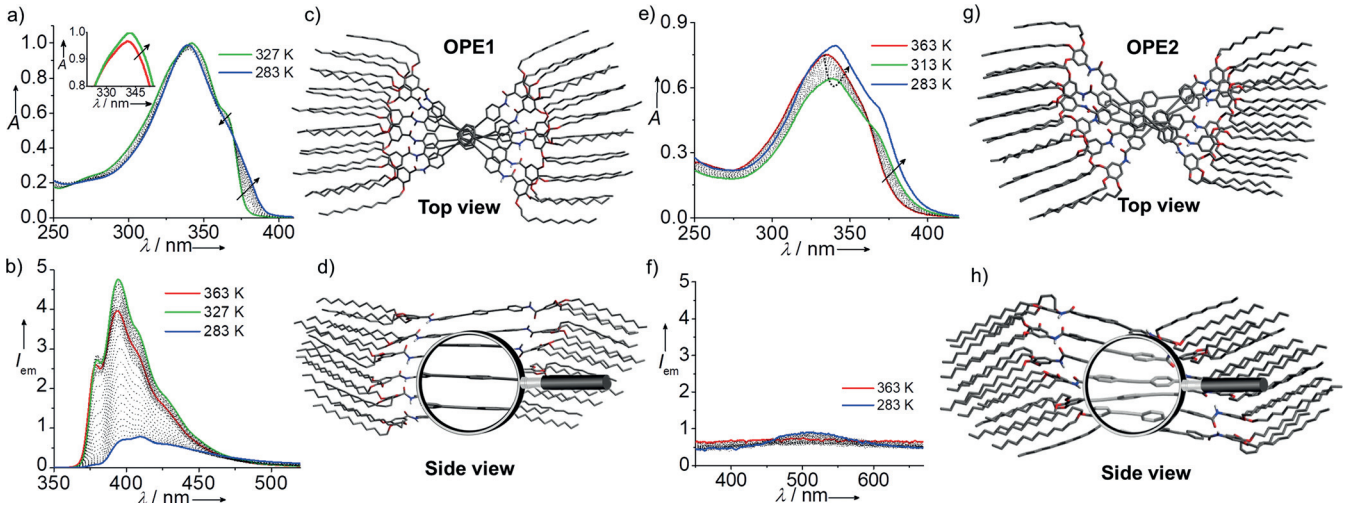

Figure 2. Temperature-dependent absorption (a, e) and emission (b, f) studies of **1** and **2** ($c = 1 \times 10^{-4}$ M, MCH), respectively. The inset shows the increase in absorbance of **1** upon cooling from 363 K (red) to 327 K (green). Top and side views of PM7-optimized hexamers of **1** (c, d) and **2** (g, h).

methodology (Figure S10). Regarding the emission properties, **2** and **4** (Figures 2 f and S9 b, respectively) are also nearly non-emissive in MCH regardless of the temperature, as already discussed.

The overall results bring to light the importance of H-bonding to promote the self-assembly of the OPE units, as also demonstrated by the fact that a previously reported derivative with the same OPE core (OPEM[11] in Figure S11) but without amide groups showed no signs of aggregation under identical conditions. Fourier transform infrared spectroscopic (FTIR) measurements for all OPEs **1**–**4** in MCH show typical values of H-bonded amide groups, that is, N–H and C=O stretching frequencies in the range of 3290-3269 cm^{-1} and 1645–1653 cm^{-1}, respectively.[12] Furthermore, lower stretching frequencies were observed in $CHCl_3$ upon cooling, indicating a strengthening in the intermolecular H-bonds upon aggregation (Figures S12–S15). This synergy between H-bonding and aromatic interactions in all OPEs is responsible for a cooperative supramolecular polymerization, as revealed by global fitting of the cooling curves (α_{agg} vs. T) extracted from UV/Vis spectra recorded at different concentrations (Figures S16 and S17 and Table S1) to the equilibrium (EQ) model.[13] For the C_2-symmetrical systems, the degree of cooperativity σ is slightly lower for the C-centered OPE **2** than for N-centered **1**, a trend that is even more pronounced for the C_3-symmetrical OPEs (≈ one order of magnitude lower for **4**, Table S1). This higher cooperativity found for our C-centered vs. N-centered systems is also in line with the behavior observed for benzenetrisamide derivatives,[3d,14] but this trend is opposite to that displayed by related C_3-symmetrical systems derived from OPE.[15] This difference may be due to the different nature of the substituents attached to the amide groups (for our systems both the C=O and the N–H groups of the amides are attached to an aromatic ring, whereas the previously reported C_3-symmetrical OPEs feature an alkyl chain attached to the amide).

In order to gain insight into the reciprocal influence of H-bonds and aromatic interactions on the evolution of the self-assembled structures, we monitored the chemical shifts of **1** and **2** by VT-^{1}H-NMR measurements in MCH-d_{14} upon cooling the monomer solutions from 363 to 283 K at 2.5×10^{-4} M. For **1**, the amide N-H signal initially shifts downfield from $\delta = 7.43$ to 7.50 ppm when the solution is cooled from 363 to 343 K, and then broadens with further decrease in temperature (Figure 3 a). In contrast, the proton signals corresponding to the peripheral phenyl rings display a less pronounced broadening with insignificant (0.01 ppm) shifts in the same temperature window. Interestingly, the signals corresponding to the central phenyl ring of the OPE core remain initially unaffected between 363 and 343 K; however, further cooling to 323 K induces a significant broadening and upfield shift. On the other hand, the doublet at 7.60 ppm

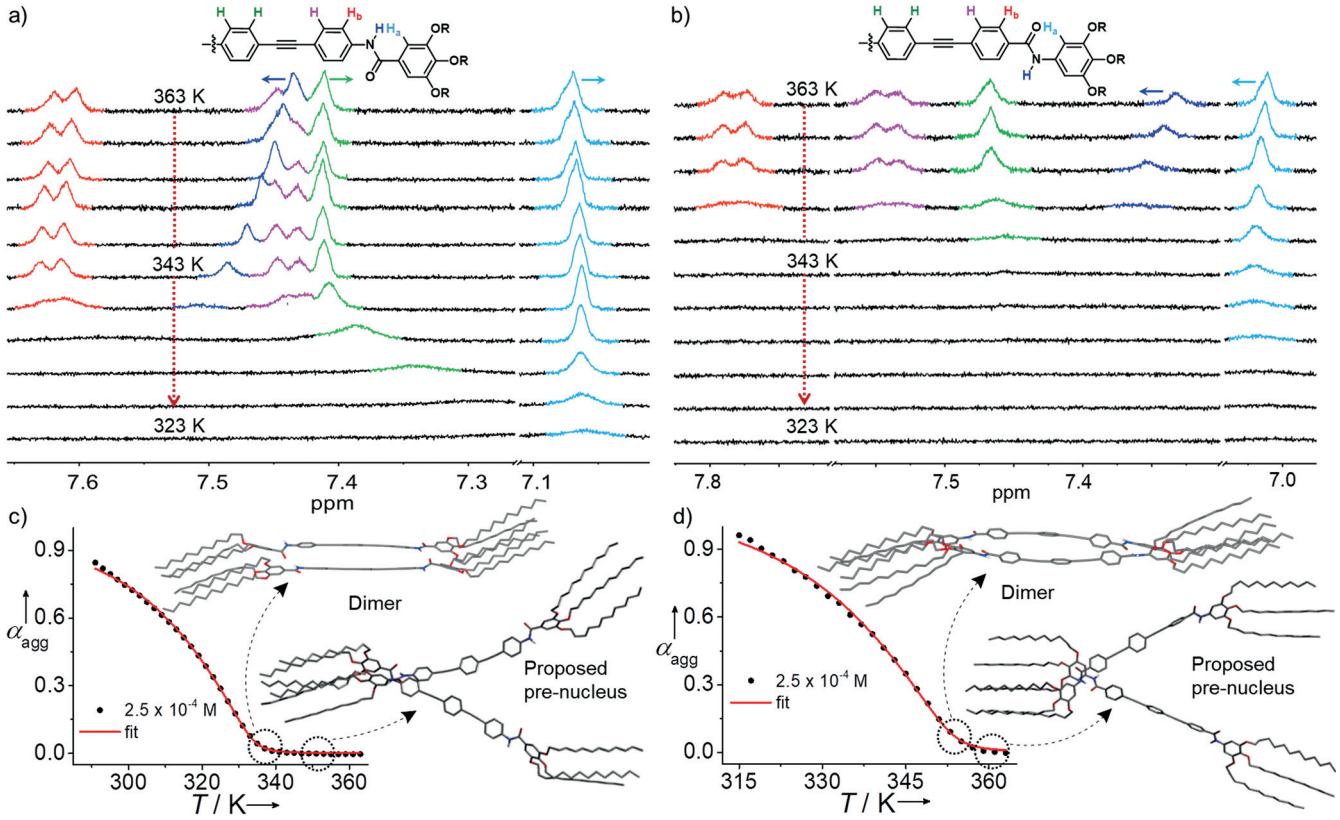

Figure 3. Sections of the variable-temperature ^{1}H-NMR spectra of **1** (a) and **2** (b) in MCH-d_{14} at 2.5×10^{-4} M. c, d) Cooling curves determined from VT-UV/Vis measurements at 2.5×10^{-4} M for **1** (c) and **2** (d) obtained by monitoring the absorbance at 385 nm and 380 nm, respectively. The geometries of the proposed prenuclei and dimer structures shown in (c) and (d) are the initial (prenucleus) and optimized (dimer) structures obtained from PM7 calculations.

undergoes a meager downfield shift between 363 and 343 K and ultimately moves upfield below 343 K due to the initiation of aggregation. These results suggest that the self-assembly process is separated into prenucleation, nucleation, and elongation phases. Analysis of the cooling curve extracted from UV/Vis studies under identical conditions affords an elongation temperature (T_e) of 334 K for **1**, which implies that the temperature range 363–343 K corresponds to the prenucleation regime (Figure 3c). In this temperature range, the amide groups are already involved in H-bonding, whereas the protons H_a and H_b slightly shift to lower and higher magnetic fields, respectively, well before the aggregation is initiated. Possibly, disorganized prenucleus dimers (we can make this assumption considering the approximation of the EQ model) are formed above T_e. A plausible explanation would be the initial association of two monomers via an H-bond through the amide groups into a V-shaped prenucleus dimer (Figure 3c, inset). Within this arrangement, only the outer phenyl ring H_a would be involved in π-stacking resulting in the observed shielding, while H_b protons might weakly interact with the carbonyl oxygen of the adjacent molecule leading to a weak downfield shift, as suggested by PM7 calculations. Cooling below 343 K promotes a molecular rearrangement into a stable, more organized nucleus dimer with a compact parallel arrangement, which acts as a seed for the supramolecular growth into twisted stacks through cooperative H-bonding and π-stacking interactions below T_e. This is supported theoretically by PM7 calculations and experimentally by the significant broadening of all NMR signals and the fact that the central OPE ring is strongly shielded and the adjacent ring is only slightly affected, while the outer ring signal remains completely unaltered. VT-^{1}H-NMR and semiempirical calculations performed for **3** gave similar trends as those found for **1** (Figure S18), although in this case $CDCl_3$ served as the solvent due to severe signal broadening in MCH-d_{14}.

For **2** under the same experimental conditions, signal broadening occurs at a higher temperature (353 K) than for **1** (343 K); this is in line with the higher calculated value of T_e (352 K) (Figure 3b,d). For the C_3-symmetrical homologues, T_e is also higher for the C-centered **4** and the NMR signals also broaden at higher T (Figure S19). With regards to the specific chemical shifts, the amide N–H signal at 7.33 ppm shifts slightly downfield to 7.36 between 363 and 353 K, while further cooling causes significant broadening and ultimate disappearance of the signal. These observations suggest a higher tendency of the C-centered monomers to associate into prenuclei, which, however, appear to have a lower stabilization through H-bonds. In contrast to **1**, the protons corresponding to the peripheral phenyl rings of **2** display only a minor downfield shift (0.01 ppm) upon cooling, while all other aromatic protons remain nearly unaffected but are likewise broadened as a result of aggregation. This might suggest that aromatic interactions negligibly influence the prenucleus formation of **2**, which is primarily stabilized by H-bonds that are weaker than those of **1**. Further cooling down to the T_e initiates the formation of a dimer nucleus, whose π-backbone is considerably more distorted than for the dimer of **1** due to less efficient H-bonding, as predicted by PM7 calculations (Figure 3d). Ultimately, the nuclei undergo further growth into higher order aggregates that are responsible for the signal broadening below 351 K. All these observations confirm a better match between the H-bonding arrangement and preorganization for **1** than for the C-centered **2**, which ultimately results in a more compact and ordered organization of the π-backbones in the supramolecular structures. This is in excellent agreement with the hydrogen bonding trends found in the theoretical calculations: the H-bonding distances are shorter for **1** aggregates (Figure S20).

This dissimilar interplay of noncovalent interactions results in distinct nanostructure morphologies for **1** and **2**, as revealed by atomic force microscopy (AFM) on highly oriented pyrolytic graphite (HOPG). While **1** self-assembles into highly entangled fibers of several microns in length, **2** forms considerably smaller round-shaped discrete aggregates (Figures 4 and S21). The individual fibers of **1** have an

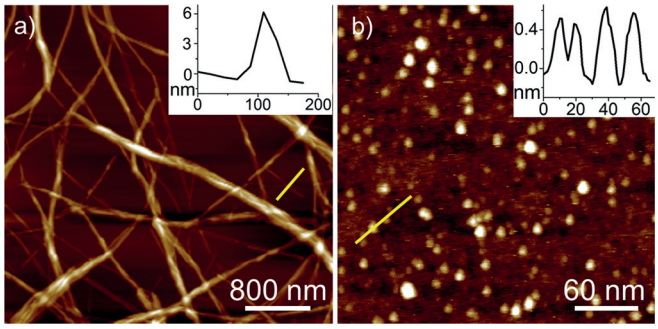

Figure 4. AFM images of **1** (a) and **2** (b) obtained by spin-coating the respective MCH solutions ($c = 5 \times 10^{-5}$ M) on HOPG with corresponding cross-section analysis along the yellow lines.

approximate height of 6.5 nm, which matches with a molecular length of ca. 6.3 nm. On the other hand, the disk-like assemblies of **2** have diameters ranging from 15 to 20 nm but a height of only 0.4–0.6 nm (inset of Figure 4b). These remarkably different height and diameter values rule out the formation of spherical objects, and suggest that the disorganized stacks of **2** are arranged edge-on on the HOPG substrate (see the side view of stacks of **2** in Figure 2h). This distortion explains why further growth of the system in a preferred direction into one-dimensional fibers is hindered. The C_3-symmetrical **3** and **4** also form long fibers and small disordered objects, respectively (Figure S22).

In conclusion, we have elucidated the reciprocal impact of H-bonding and preorganization on the evolution of supramolecular systems by detailed analysis of the changes in molecular conformation preceding aggregation. This was achieved by comparison of appropriate C_2- and C_3-symmetrical OPE systems that exclusively differ in the amide topology. Various experiments and theory reveal how this subtle structural change brings about differences in their photophysical and supramolecular properties, such as molecular packing and aggregate morphology. Our understanding of the subtle interplay of different noncovalent interactions in self-assembled structures might serve as a stepping stone for the rational design of molecular systems that can evolve via intricate processes into functional superstructures.

Acknowledgements

We acknowledge the Humboldt Foundation (Sofja-Kovalevskaja Award) and the European Commission (SUPRACOP ERC-StG-2016) for funding.

Conflict of interest

The authors declare no conflict of interest.

Keywords: hydrogen bonds · oligophenyleneethynylene · π-conjugated systems · π–π interactions · self-assembly

How to cite: *Angew. Chem. Int. Ed.* **2019**, *58*, 4732 – 4736
Angew. Chem. **2019**, *131*, 4782 – 4787

[1] a) G. M. Whitesides, B. Grzybowski, *Science* **2002**, *295*, 2418 – 2421; b) J. Černý, P. Hobza, *Phys. Chem. Chem. Phys.* **2007**, *9*, 5291 – 5303; c) D. A. Uhlenheuer, K. Petkau, L. Brunsveld, *Chem. Soc. Rev.* **2010**, *39*, 2817 – 2826.

[2] a) D. González-Rodríguez, A. P. H. J. Schenning, *Chem. Mater.* **2011**, *23*, 310 – 325; b) M. R. Molla, S. Ghosh, *Chem. Mater.* **2011**, *23*, 95 – 105; c) T. Aida, E. W. Meijer, S. I. Stupp, *Science* **2012**, *335*, 813 – 817; d) M. R. Molla, S. Ghosh, *Phys. Chem. Chem. Phys.* **2014**, *16*, 26672 – 26683; e) C. Rest, R. Kandanelli, G. Fernández, *Chem. Soc. Rev.* **2015**, *44*, 2543 – 2572; f) S. Yagai, *Bull. Chem. Soc. Jpn.* **2015**, *88*, 28 – 58; g) A. Das, S. Ghosh, *Chem. Commun.* **2016**, *52*, 6860 – 6872; h) F. Würthner, C. R. Saha-Möller, B. Fimmel, S. Ogi, P. Leowanawat, D. Schmidt, *Chem. Rev.* **2016**, *116*, 962 – 1052; i) J.-M. Lehn, *Chem. Soc. Rev.* **2017**, *46*, 2378 – 2379; j) B. Adhikari, X. Lin, M. Yamauchi, H. Ouchi, K. Aratsu, S. Yagai, *Chem. Commun.* **2017**, *53*, 9663 – 9683; k) P. Pramanik, D. Ray, V. K. Aswal, S. Ghosh, *Angew. Chem. Int. Ed.* **2017**, *56*, 3516 – 3520; *Angew. Chem.* **2017**, *129*, 3570 – 3574; l) D. S. Pal, H. Kar, S. Ghosh, *Chem. Commun.* **2018**, *54*, 928 – 931.

[3] a) T. F. A. De Greef, M. M. J. Smulders, M. Wolffs, A. P. H. J. Schenning, R. P. Sijbesma, E. W. Meijer, *Chem. Rev.* **2009**, *109*, 5687 – 5754; b) C. Kulkarni, S. Balasubramanian, S. J. George, *ChemPhysChem* **2013**, *14*, 661 – 673; c) P. A. Korevaar, T. F. A. de Greef, E. W. Meijer, *Chem. Mater.* **2014**, *26*, 576 – 586; d) C. Kulkarni, E. W. Meijer, A. R. A. Palmans, *Acc. Chem. Res.* **2017**, *50*, 1928 – 1936; e) I. V. Kolesnichenko, E. V. Anslyn, *Chem. Soc. Rev.* **2017**, *46*, 2385 – 2390; f) D. B. Amabilino, D. K. Smith, J. W. Steed, *Chem. Soc. Rev.* **2017**, *46*, 2404 – 2420; g) H. Wang, Z. Feng, B. Xu, *Chem. Soc. Rev.* **2017**, *46*, 2421 – 2436; h) S. Dhiman, S. J. George, *Bull. Chem. Soc. Jpn.* **2018**, *91*, 687 – 699.

[4] S. S. Babu, V. K. Praveen, A. Ajayaghosh, *Chem. Rev.* **2014**, *114*, 1973 – 2129.

[5] a) Y. Yamaguchi, S. Kobayashi, T. Wakamiya, Y. Matsubara, Z. Yoshida, *Angew. Chem. Int. Ed.* **2005**, *44*, 7040 – 7044; *Angew. Chem.* **2005**, *117*, 7202 – 7206; b) A. P. H. J. Schenning, E. W. Meijer, *Chem. Commun.* **2005**, 3245 – 3258; c) Y. Yamaguchi, T. Ochi, S. Miyamura, T. Tanaka, S. Kobayashi, T. Wakamiya, Y. Matsubara, Z. Yoshida, *J. Am. Chem. Soc.* **2006**, *128*, 4504 – 4505.

[6] a) A. J. Zucchero, P. L. McGrier, U. H. F. Bunz, *Acc. Chem. Res.* **2010**, *43*, 397 – 408; b) U. H. F. Bunz, K. Seehafer, M. Bender, M. Porz, *Chem. Soc. Rev.* **2015**, *44*, 4322 – 4336.

[7] S. Höger, D. L. Morrison, V. Enkelmann, *J. Am. Chem. Soc.* **2002**, *124*, 6734 – 6736.

[8] a) S. Yagai, S. Mahesh, Y. Kikkawa, K. Unoike, T. Karatsu, A. Kitamura, A. Ajayaghosh, *Angew. Chem. Int. Ed.* **2008**, *47*, 4691 – 4694; *Angew. Chem.* **2008**, *120*, 4769 – 4772; b) S. Mahesh, R. Thirumalai, S. Yagai, A. Kitamura, A. Ajayaghosh, *Chem. Commun.* **2009**, 5984 – 5986; c) A. Gopal, R. Varghese, A. Ajayaghosh, *Chem. Asian J.* **2012**, *7*, 2061 – 2067; d) F. García, L. Sánchez, *J. Am. Chem. Soc.* **2012**, *134*, 734 – 742; e) F. Wang, M. A. J. Gillissen, P. J. M. Stals, A. R. A. Palmans, E. W. Meijer, *Chem. Eur. J.* **2012**, *18*, 11761 – 11770; f) F. Aparicio, F. García, L. Sánchez, *Chem. Eur. J.* **2013**, *19*, 3239 – 3248; g) S. K. Albert, H. V. P. Thelu, M. Golla, N. Krishnan, S. Chaudhary, R. Varghese, *Angew. Chem. Int. Ed.* **2014**, *53*, 8352 – 8357; *Angew. Chem.* **2014**, *126*, 8492 – 8497; h) H. V. P. Thelu, S. K. Albert, M. Golla, N. Krishnan, S. B. Yamijala, S. V. Nair, S. M. Srinivasula, R. Varghese, *ChemistrySelect* **2016**, *1*, 5389 – 5396; i) J. Buendía, F. García, B. Yelamos, L. Sánchez, *Chem. Commun.* **2016**, *52*, 8830 – 8833; j) S. K. Albert, M. Golla, H. V. P. Thelu, N. Krishnan, R. Varghese, *Chem. Eur. J.* **2017**, *23*, 8348 – 8352; k) M. Hifsudheen, R. K. Mishra, B. Vedhanarayanan, V. K. Praveen, A. Ajayaghosh, *Angew. Chem. Int. Ed.* **2017**, *56*, 12634 – 12638; *Angew. Chem.* **2017**, *129*, 12808 – 12812.

[9] a) A. Slama-Schwok, M. Blanchard-Desce, J. M. Lehn, *J. Phys. Chem.* **1990**, *94*, 3894 – 3902; b) S.-Y. Kim, Y.-J. Cho, A.-R. Lee, H.-j. Son, W.-S. Han, D. W. Cho, S. O. Kang, *Phys. Chem. Chem. Phys.* **2017**, *19*, 426 – 435.

[10] a) M. Levitus, K. Schmieder, H. Ricks, K. D. Shimizu, U. H. F. Bunz, M. A. Garcia-Garibay, *J. Am. Chem. Soc.* **2001**, *123*, 4259 – 4265; b) M. I. Sluch, A. Godt, U. H. F. Bunz, M. A. Berg, *J. Am. Chem. Soc.* **2001**, *123*, 6447 – 6448; c) P. V. James, P. K. Sudeep, C. H. Suresh, K. G. Thomas, *J. Phys. Chem. A* **2006**, *110*, 4329 – 4337; d) U. H. F. Bunz, *Macromol. Rapid Commun.* **2009**, *30*, 772 – 805; e) K. Seehafer, M. Bender, U. H. F. Bunz, *Macromolecules* **2014**, *47*, 922 – 927.

[11] M. J. Mayoral, C. Rest, J. Schellheimer, V. Stepanenko, G. Fernández, *Chem. Eur. J.* **2012**, *18*, 15607 – 15611.

[12] a) S. Ogi, K. Sugiyasu, S. Manna, S. Samitsu, M. Takeuchi, *Nat. Chem.* **2014**, *6*, 188 – 195; b) S. Ogi, V. Stepanenko, K. Sugiyasu, M. Takeuchi, F. Würthner, *J. Am. Chem. Soc.* **2015**, *137*, 3300 – 3307.

[13] H. M. M. ten Eikelder, A. J. Markvoort, T. F. A. de Greef, P. A. J. Hilbers, *J. Phys. Chem. B* **2012**, *116*, 5291 – 5301.

[14] a) P. J. M. Stals, J. C. Everts, R. d. Bruijn, I. A. W. Filot, M. M. J. Smulders, R. Martín-Rapún, E. A. Pidko, T. F. A. de Greef, A. R. A. Palmans, E. W. Meijer, *Chem. Eur. J.* **2010**, *16*, 810 – 821; b) R. Q. Albuquerque, A. Timme, R. Kress, J. Senker, H.-W. Schmidt, *Chem. Eur. J.* **2013**, *19*, 1647 – 1657; c) M. P. Oliveira, H. W. Schmidt, R. Q. Albuquerque, *Chem. Eur. J.* **2018**, *24*, 2609 – 2617.

[15] F. García, J. Arago, P. M. Viruela, E. Orti, L. Sánchez, *Chem. Commun.* **2016**, *52*, 6907 – 6910.

Manuscript received: December 7, 2018
Accepted manuscript online: January 8, 2019
Version of record online: March 3, 2019

